Valverde-Muñoz, FJ.; Muñoz Roca, MDC.; Ferrer, S.; Bartual-Murgui, C.; Real, JA. (2018). Switchable Spin-Crossover Hofmann-Type 3D Coordination Polymers Based on Tri- and Tetratopic Ligands. Inorganic Chemistry. 57(19):12195-12205. https://doi.org/10.1021/acs.inorgchem.8b01842

Switchable Spin-Crossover Hofmann-Type 3D Coordination Polymers Based on Tri- and Tetratopic Ligands

Francisco Javier Valverde-Muñoz,[†] M. Carmen Muñoz,[‡] Sacramento Ferrer,[§] Carlos Bartual-Murgui,[†] and Jose A. Real*[,†]

[†]Institut de Ciència Molecular (ICMol), Universitat de València, C/Catedrático José Beltrán Martínez, 2, 46980 Paterna, Valencia, Spain

[‡]Departamento de Física Aplicada, Universitat Politècnica de València, Camino de Vera s/n, 46022 Valencia, Spain

[§]Departament de Química Inorgànica, Universitat de València, Av. Vicent Andrés Estellés, s/n, 46100 Burjassot, Valencia, Spain

*Supporting Information

ABSTRACT: Fe^{II} spin-crossover (SCO) coordination polymers of the Hofmann type have become an archetypal class of responsive materials. Almost invariably, the construction of their architectures has been based on the use of monotopic and linear ditopic pyridine-like ligands. In the search for new Hofmann-type architectures with SCO properties, here we analyze the possibilities of bridging ligands with higher connectivity degree. More precisely, the synthesis and structure of $\{Fe^{II}(L^{N3})[M^{I}(CN)_2]_2\}\cdot$(Guest) (Guest = nitrobenzene, benzonitrile, *o*-dichlorobenzene; M^{I} = Ag, Au) and $\{Fe^{II}(L^{N4})[Ag_2(CN)_3][Ag(CN)_2]\}\cdot H_2O$ are described, where L^{N3} and L^{N4} are the tritopic and tetratopic ligands 1,3,5-tris(pyridin-4-ylethynyl)benzene and 1,2,4,5-tetrakis(pyridin-4-ylethynyl)benzene. This new series of Hofmann clathrates displays thermo- and photoinduced SCO behaviors.

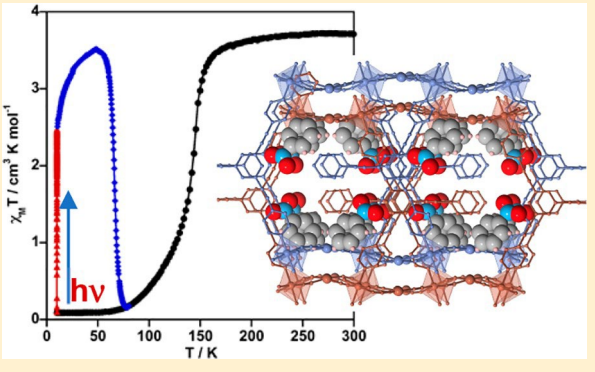

INTRODUCTION

Iron(II) spin-crossover (SCO) complexes are remarkable types of responsive molecular materials that can be reversibly switched between the electronic high-spin (HS) and low-spin (LS) states in response to environmental stimuli, such as temperature, pressure, light irradiation, and analytes.[1] The LS ↔ HS switch is manifested by reversible, controllable, and detectable changes in the physicochemical properties (optical, magnetic, electrical, and structural), making these functional molecular materials excellent prototypes of sensors, switches, and memories.[2]

Within the so-called polymeric approach to the synthesis of Fe^{II} SCO compounds, Hofmann-type coordination polymers have been gaining considerable attention in the past decade and now they constitute an archetypal family in the SCO area.[3] They are a class of two- and three-dimensional cyanide-bridged bimetallic compounds formulated as $\{Fe^{II}(L)_x[M^{II}(CN)_4]\}_n$, where M^{II} is Ni, Pd, or Pt and L can be an N-donor monodentate (x = 2) or bis-monodentate rodlike (x = 1) ligand. The structure is invariably constituted of parallel stacks of two-dimensional $\{Fe^{II}[M^{II}(CN)_4]\}_n$ square grids in which Fe^{II} is equatorially coordinated to four $[M^{II}(CN)_4]^{2-}$ planar units through the N atom while the axial positions are occupied by two L ligands, defining two-dimensional (2D)[4] or three-dimensional (3D)[5] coordination polymers when L is a terminal monodentate or a bis-monodentate bridging ligand, respectively. The latter connects the M^{II} centers of consecutive layers, thus generating bifunctional porous fsc (RCSR database) frameworks in which SCO properties and host−guest chemistry interplay in a synergetic way.[5f−h,6]

Coordination polymers with the formula $\{Fe^{II}(L)_x[M^{I}(CN)_2]_2\}_n$, where M^{I} = Cu, Ag, Au, are usually included in the family of Hofmann-type compounds. The Fe^{II} sites can be structurally described in the same terms as for $\{Fe^{II}(L)_x[M^{II}(CN)_4]\}_n$. However, the linear bis-monodentate rodlike $[M^{I}(CN)_2]^-$ bridges produce more open frameworks with pcu topology, which usually favor double, triple, and even quadruple interpenetration of the frameworks.[3a,c] At variance with $\{Fe^{II}(L)_2[M^{II}(CN)_4]\}_n$, which only form 2D frameworks, monodentate L ligands can also form 3D frameworks with more varied topologies (e.g., nbo and cds among others).[7] Usually, the $\{Fe^{II}(L)_x[M^{I}(CN)_2]_2\}_n$ frameworks interact with each other through short $M^{I}\cdots M^{I}$ metallophilic contacts. Furthermore, the susceptibility of M^{I}−(Cu,Ag) to expand the coordination sphere or generate oligomers (e.g., $[Ag_2(CN)_3]^-$) also adds interesting features to this subfamily of compounds.

Hofmann-type Fe^{II} SCO coordination polymers have afforded excellent examples of thermo- and piezohysteretic behaviors, multistep cooperative transitions, relevant examples

DOI:

Scheme 1. Organic Bridging Ligands Used in This Work

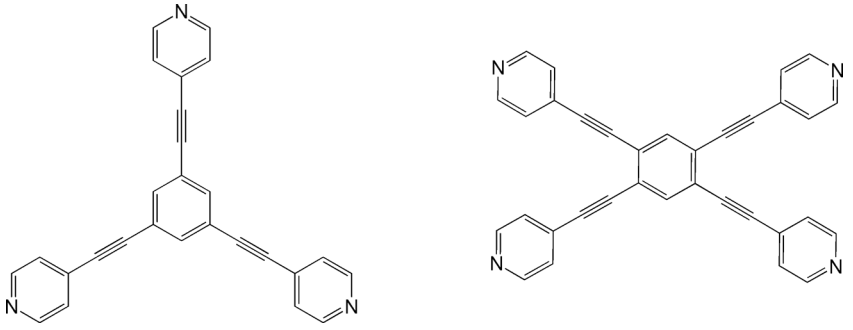

Table 1. Crystallographic Parameters for 1·$PhNO_2$, 2·$PhNO_2$, and 3·H_2O

	1·$PhNO_2$		2·$PhNO_2$		3·H_2O	
	120 K	250 K	100 K	250 K	120 K	250 K
empirical formula	$C_{37}H_{20}Ag_2FeN_8O_2$		$C_{37}H_{20}Au_2FeN_8O_2$		$C_{39}H_{18}Ag_3FeN_9O$	
M_r	880.20		1058.39		008.08	
cryst syst	orthorhombic		orthorhombic		triclinic	
space group	*Pbcn*		*Pbcn*		$P\bar{1}$	
a (Å)	36.5834(10)	36.806(2)	36.7927(12)	36.931(2)	7.9977(5)	7.9807(5)
b (Å)	15.2354(4)	15.8826(5)	15.1716(5)	15.6980(4)	9.5996(9)	9.8952(6)
c (Å)	13.2204(3)	13.4475(5)	13.1200(4)	13.3384(4)	13.5845(5)	13.8305(8)
α (deg)					89.642(5)	89.434(4)
β (deg)					80.717(5)	80.842(5)
γ (deg)					71.166(7)	71.898(5)
V (Å^3)	7368.6(3)	7861.0(5)	7323.6(4)	7732.8(4)	973.00(12)	1024.00(11)
Z	8	8	8	8	1	1
F(000)	3472		3984		490	
D_c (mg cm^{-3})	1.587	1.487	1.920	1.818	1.720	1.661
μ(Mo Kα) (mm^{-1})	1.484	1.391	8.427	7.982	1.895	1.804
total no. of rflns ($I > 2\sigma(I)$)	7681	5381	7739	6638	3694	3496
R ($I > 2\sigma(I)$)	0.0681	0.0672	0.0383	0.0463	0.0609	0.0670
R_w ($I > 2\sigma(I)$)	0.1453	0.1674	0.0905	0.0859	0.1569	0.1776
S	1.068	1.014	1.033	1.066	1.046	1.050

of porous systems where the SCO behavior can be tuned by guest molecules favoring selective host−guest interactions, catalytic activity, and/or solid-state transformations.[8] In addition, these compounds are excellent platforms to investigate the SCO properties at the nanoscale (nanocrystals, thin films)[5b,9] and their potential application as prototypes of spintronic and micromechanical devices.[10] Thus, the design and synthesis of new Hofmann-type Fe^{II} SCO compounds are essential steps for discovering new, interesting properties and applications. In this respect, almost all Hofmann-type Fe^{II} SCO compounds so far investigated have been prepared from mono- and ditopic L ligands. Indeed, as far as we know, the only exception corresponds to the porous coordination polymers $\{Fe(TPT)_{2/3}[M^I(CN)_2]_2\}\cdot n$(Guest), where TPT is 2,4,6-tris(4-pyridyl)-1,3,5-triazine, a tritopic ligand with D_{3h} symmetry.[11]

As a further step in this study, herein we report on the synthesis and characterization of two unprecedented series of Fe^{II} SCO coordination polymers based on the tritopic and tetratopic ligands L^{N3} = 1,3,5-tris(pyridin-4-ylethynyl)benzene and L^{N4} = 1,2,4,5-tetrakis(pyridin-4-ylethynyl)benzene (Scheme 1) and ditopic $[M^I(CN)_2]^-$ inorganic bridges. The L^{N3} ligand is an expanded version of the previously investigated TPT ligand, while the topology of the L^{N4} ligand is investigated for the first time in the family of Hofmann clathrates. More precisely, we will present the crystal structures and magnetic and photomagnetic properties of $\{Fe^{II}(L^{N3})[M^I(CN)_2]_2\}\cdot$(Guest) ($M^I$ = Ag (1·Guest), M^I = Au (2·Guest); Guest = C_6H_5X (X = NO_2, CN), *o*-$C_6H_4Cl_2$)) and $\{Fe^{II}(L^{N4})[Ag_2(CN)_3][Ag(CN)_2]\}\cdot H_2O$ (3·H_2O).

RESULTS

Synthesis. The synthesis of the title compounds was conditioned by the high insolubility of the ligands L^{N3} and L^{N4} and the resulting coordination polymers. Thus, in order to get reasonably good microcrystalline samples and single crystals of 1·Guest, 2·Guest, and 3·H_2O, the synthesis was carried out by slow diffusion of the components (see also the Experimental Section). The presence of guest molecules was an additional key condition for the synthesis of complexes with L^{N3}. Thus, we found that the use of an H-type diffusion system made up of four connected vessels resulted in the most appropriate strategy. In such a configuration, methanolic solutions of Fe^{II} and $[M(CN)_2]^-$ were poured separately into the peripheral vessels, while L_{N3} was placed as a solid (due to its insolubility) at the bottom of the vessel next to the Fe^{II} solution, and a large excess of Guest was placed in the remainder vessel. Alternatively, to slow the diffusion, it is also possible to add the Fe^{II} and $[M(CN)_2]^-$ salts as solids at the bottom of the corresponding tubes. Finally, the four vessels were filled with

Table 2. Selected Bond Lengths (Å) for 1·$PhNO_2$, 2·$PhNO_2$, and 3·H_2O

	1·$PhNO_2$		2·$PhNO_2$		3·H_2O	
	120 K	250 K	100 K	250 K	120 K	250 K
Fe−N1	2.033(4)	2.217(6)	2.048(5)	2.220(5)	2.045(4)	2.241(4)
Fe−N2	2.046(4)	2.228(5)	2.061(5)	2.217(5)	1.955(4)	2.117(5)
Fe−N3	1.968(4)	2.166(5)	1.975(5)	2.157(6)	1.957(4)	2.141(5)
Fe−N4	1.969(4)	2.145(5)	1.994(5)	2.148(5)		
Fe−N5	1.971(5)	2.151(5)	1.982(5)	2.149(6)		
Fe−N6	1.973(5)	2.151(5)	1.986(5)	2.154(6)		
Ag1−C28	2.043(5)	2.031(6)				
Ag1−C29	2.044(5)	2.049(6)				
Ag2−C30	2.053(6)	2.052(6)				
Ag2−C31	2.059(6)	2.060(6)				
Au1−C28			1.986(6)	1.987(7)		
Au1−C29			1.970(6)	1.982(7)		
Au2−C30			1.989(7)	1.989(7)		
Au2−C31			1.983(6)	1.977(6)		
Au1−Au2			3.268(1)	3.270(1)		
Ag1−N4					2.435(4)	2.470(6)
Ag1−N5					2.119(5)	2.095(7)
Ag1−C18					2.068(5)	2.054(6)
Ag1−C19					2.119(5)	2.095(7)
Ag2−C20					2.058(5)	2.060(6)
Ag1−Ag2	3.275(1)	3.247(1)				

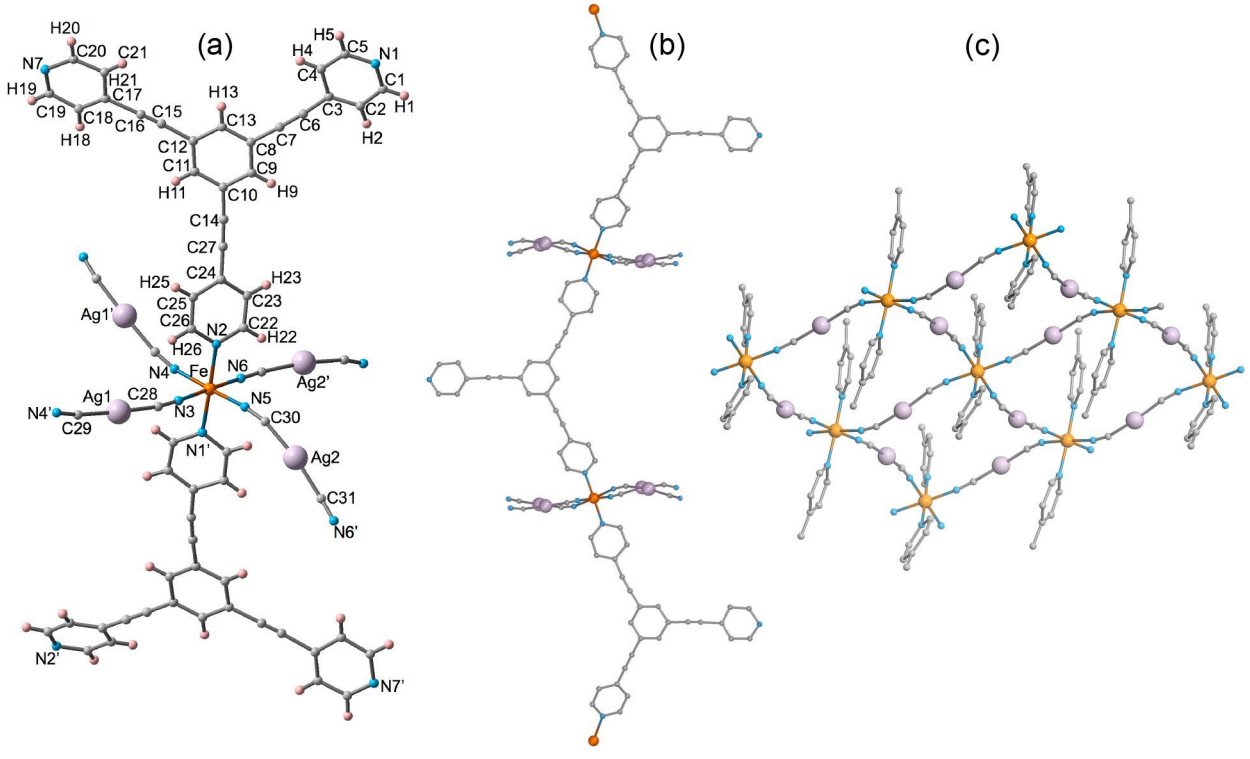

Figure 1. (a) Coordination center of 1·$PhNO_2$ at 120 K showing the atom labeling of the asymmetric unit (the atom labeling for the Au derivative (2·$PhNO_2$) is the same). (b) Fragment of the zigzag chain running along [100]. (c) $\{Fe_4[M^I(CN)_2]_4\}$ corrugated 2D grids.

methanol and sealed (Figure S1). The most appropriate guest molecules turned out to be the following benzene derivatives: $PhNO_2$, *o*-$PhCl_2$, and PhCN. In contrast, the use of five-membered rings as guests, i.e. pyrrole, furan, and thiophene, was unsuccessful and no product was formed. PXRD patterns for the 1·Guest and 2·Guest series are practically identical, demonstrating their isostructural nature (Figure S2). Despite the high crystallinity of these compounds, adequate single crystals to get reasonably good structural X-ray diffraction analyses were achieved only for 1·$PhNO_2$ and 2·$PhNO_2$.

Given that L^{N4} is soluble in $CHCl_3$ and that the structure of 3·H_2O cannot accept guest molecules (vide infra), a three-vessel modification was employed (see Figure S1). At variance with 3·H_2O, self-assembly of Fe^{II}, L^{N4}, and $[Au(CN)_2]^-$ does not give any type of complex even in the presence of guest molecules. This may be due to metric and/or geometric

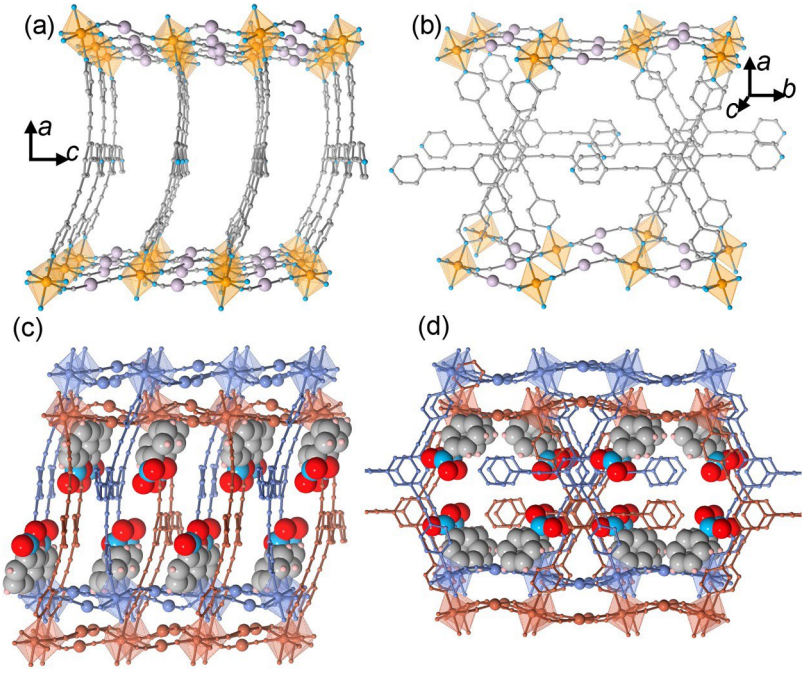

Figure 2. Perspective views of a fragment of the 3D framework of 1·$PhNO_2$ at 120 K: a single framework running along the [001] (a) and [010] (b) directions and the same perspectives showing the double-interpenetrated frameworks loaded with $PhNO_2$ (c, d).

incompatibilities between connectors and nodes and the fact that the Au atom cannot expand the coordination sphere as Ag does in the case of 3·H_2O (vide infra).

The thermogravimetric analysis (TGA) for 1·Guest, 2·Guest, and 3·H_2O confirmed the amount of guest molecules (Figure S3). The TGA for fresh samples of 1·$PhNO_2$ and 2·$PhNO_2$ shows, prior to the loss of the $PhNO_2$ molecule, a quite small weight loss (ca. 0.5 and 0.3%, respectively) on starting from room temperature, which could be tentatively associated with the presence of a quite small amount of methanol. Because the amount of these molecules is less than ca. 1/8 CH_3OH and these species are very labile, we have considered that, under vacuum conditions of the SQUID magnetometer or even under ambient storage conditions, these molecules spontaneously desolvate, as suggested by the structure analysis and the magnetic properties (vide infra). The average yields for 1·Guest and 2·Guest were ca. 15−20%, and that of 3·H_2O was 10−15%.

Structure. The crystal structure was determined by single-crystal X-ray analysis at 120 and 250 K for 1·$PhNO_2$ and 3·H_2O and at 100 and 250 K for 2·$PhNO_2$. Compounds 1·$PhNO_2$ and 2·$PhNO_2$ crystallize in the orthorhombic *Pbcn* space group, while compound 3·H_2O crystallizes in the triclinic $P\bar{1}$ space group. Relevant crystallographic parameters are shown in Table 1. Selected significant bond lengths and angles are given in Table 2 and Table S1, respectively.

Structures of 1·PhNO₂ and 2·PhNO₂. Given that 1·$PhNO_2$ and 2·$PhNO_2$ are isostructural, we will describe their structures simultaneously. There is a crystallographically unique Fe^{II} site that is situated in the center of a slightly elongated [FeN_6] octahedron. Figure 1 displays the coordination sphere of the Fe^{II} with the atom labeling of the asymmetric unit, which is the same for 1·$PhNO_2$ and 2·$PhNO_2$. The axial positions (Fe−N1 and Fe−N2), occupied by the pyridine moieties of the ligand L^{N3}, are about 3% longer than the equatorial positions. The four equatorial positions are occupied by two crystallographically distinct $[M^I(CN)_2]^-$ groups (Ag1/2 and Au1/2). The average ⟨[FeN_6]⟩ bond lengths are 1.993(5) [2.176(5)] Å for 1·$PhNO_2$ at 120 K [250 K] and 2.008(5) Å [2.174(6)] Å for 2·$PhNO_2$ at 100 K [250 K]. The difference values ΔR between high- and low-temperature forms equal to 0.183 Å (1·$PhNO_2$) and 0.166 Å (2·$PhNO_2$) are in agreement with the magnetic data and are consistent with the occurrence of a practically complete SCO transition for 1·$PhNO_2$ and 90% conversion at 100 K for 2·$PhNO_2$. It is worth stressing at this point that, when single crystals of the latter compound are selected directly from the mother liquor and cooled to 120 K, the crystal parameters and Fe−N bond lengths are similar to those obtained at 250 K and are consistent with the results obtained from the magnetic data measured in solution: namely, that 2·$PhNO_2$ remains in the HS state (vide infra) (see Table S2). Consistent with the TGA, this notable difference suggests the presence of very small amounts of strongly disordered labile methanol molecules included in the structure (ca. less than 0.2 molecule) at 120 K. Indeed, there is some nonassigned electron density within the cavities of the structure. An analysis using PLATON shows the occurrence of a void volume of 2 × 67 $Å^3$ centered at (0.0, 0.72, 0.25) close (ca. 2.7 Å) to the uncoordinated N7 atom. No such behavior was observed for the single-crystal study of 1·$PhNO_2$.

The sums of deviations from the ideal octahedron of the 12 "cis" N−Fe−N angles ($\sum = \sum_{i=1}^{12} |\theta - 90|$) are respectively 17.3° [26.8°] and 24.1° [25.3°] for 1·$PhNO_2$ and 2·$PhNO_2$ at 120 K [250 K], confirming that the [FeN_6] site is weakly distorted, whatever the spin state of the Fe^{II} centers. The average Fe−N−C(M^I) angles separate from 180° by 15.4° (250 K) and 10.2° (120 K) for Fe−N−C(Ag) and 16.8° (250 K) and 11.7° (100 K) for Fe−N−C(Au). Similarly, the average M^I−C−N angles deviate from linearity by 6.5° (250 K) and 10.6° (120 K) for $[Ag(CN)_2]^-$ and 4.6° (250 K) and 7.4° (100 K) for $[Au(CN)_2]^-$.

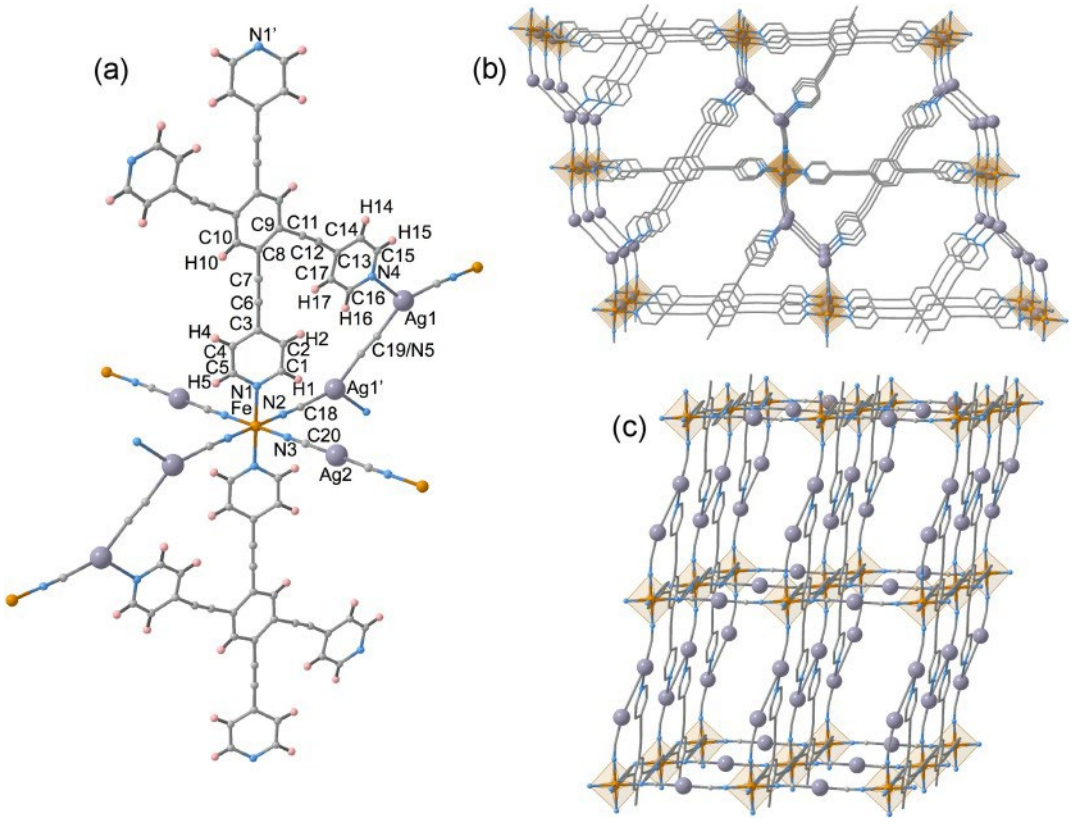

Figure 3. Coordination center of 3·H_2O at 120 K showing the atom labeling of the asymmetric unit (a). Perspective views of a fragment of the 3D framework of 3·H_2O at 120 K: two perspectives of the same fragment of a single framework emphasizing the coordination mode of L^{N4} and $[Ag_2(CN)_3]^-$ bridges (b) and the connection of the formed layers via $[Ag(CN)_2]^-$ ligands (c).

The L^{N3} ligand is not completely flat. Indeed, the mean planes defined by the pyridine moieties containing N1, N7, and N2 define angles with respect to the mean plane containing the benzene ring equal to 4.7° (4.2°), 18.9° (26.9°), and 5.4° (13.6°) for 1·$PhNO_2$ at 120 (250) K and 4.6° (4.2°), 18.9° (29.1°), and 5.1° (6.8°) for 2·$PhNO_2$ at 100 (250) K, respectively. It is noteworthy to stress the strong dependence of the angles defined by N2 and N7 on the spin state of the Fe^{II}. Furthermore, the pyridine−benzene connectors deviate slightly from linearity (by 5−6°). The pyridyl group containing the N7 atom does not coordinate either the Fe^{II} or M^I ion and is strongly disordered. Consequently, L^{N3} acts as a ditopic ligand, thereby defining zigzag chains running along [100]. In addition, the $[M^I(CN)_2]^-$ linkers radiate almost perpendicularly to the [100] direction connecting the Fe^{II} centers of four adjacent zigzag chains. Alternatively, the structure can be seen as a parallel stack of slightly corrugated 2D grids $\{Fe_4[M^I(CN)_2]_4\}$ connected by L^{N3}. The distances between two Fe^{II} centers of consecutive layers connected by L^{N3} are 18.466(1) Å at 120 K for 1·$PhNO_2$ and 18.396(2) Å at 100 K for 2·$PhNO_2$. The resulting 3D network generates enough empty room so as to favor interpenetration of two identical networks (Figure 2). The frameworks interact with each other through weak metallophilic $M^I\cdots M^I$ interactions (see Table 2) but, more importantly, through the L^{N3} ligands, which stack along the *c* direction, generating a large number of intermolecular $C\cdots C$ π short contacts smaller than the sum of the van der Waals radii (ca. 3.7 Å). These contacts increase in number and intensity when the compound moves from the HS state to the LS state (see Figures S4 and S5 and Table S3). Despite this fact, the interpenetrating frameworks generate room for inclusion of one $PhNO_2$ molecule, which are located between the L^{N3} ligands (Figure 2) and define strong π interactions with one of the pyridine rings coordinated to the Fe^{II} centers, while the other coordinated pyridine group also interacts via π with the central benzene ring of a L^{N3} ligand belonging to the adjacent framework (see Figures S4 and S5).

Structure of 3·H_2O. Figure 3 displays a fragment of the structure of 3·H_2O at 120 K together with the atom labeling of the asymmetric unit. There is one crystallographically unique $[FeN_6]$ site which lies in an inversion center defining a slightly elongated octahedron. The axial bond lengths are occupied by the pyridine moieties of the L^{N4} ligand (Fe−N1), while the four equatorial positions are occupied by $[Ag(CN)_2]^-$ and $[Ag_2(CN)_3]^-$ units through the Fe−N2 and Fe−N3 bonds. The $\langle[FeN_6]\rangle$ values equal to 1.986(4) and 2.166(4) Å at 120 and 250 K, respectively, indicate that the Fe^{II} centers are essentially in the LS and HS spin states according to the magnetic data. In this case the angular distortions of the $[FeN_6]$ octahedron, $\sum^{120\ K} = 6.9(2)°$ and $\sum^{250\ K} = 5.0(2)°$, are remarkably smaller than those in the case of 1·$PhNO_2$ and 2·$PhNO_2$.

The L^{N4} ligand is essentially flat, but the pyridine moiety bearing the N1 atom is rotated 27.1° with respect to the plane defined by the central benzene ring, which also lies in an inversion center. The Ag site in the $[Ag(CN)_2]^-$ unit is strictly linear. In contrast, the Ag site in the in situ generated $[Ag_2(CN)_3]^-$ species expands the coordination sphere to 3, affording a distorted-trigonal geometry. The trigonal geometry

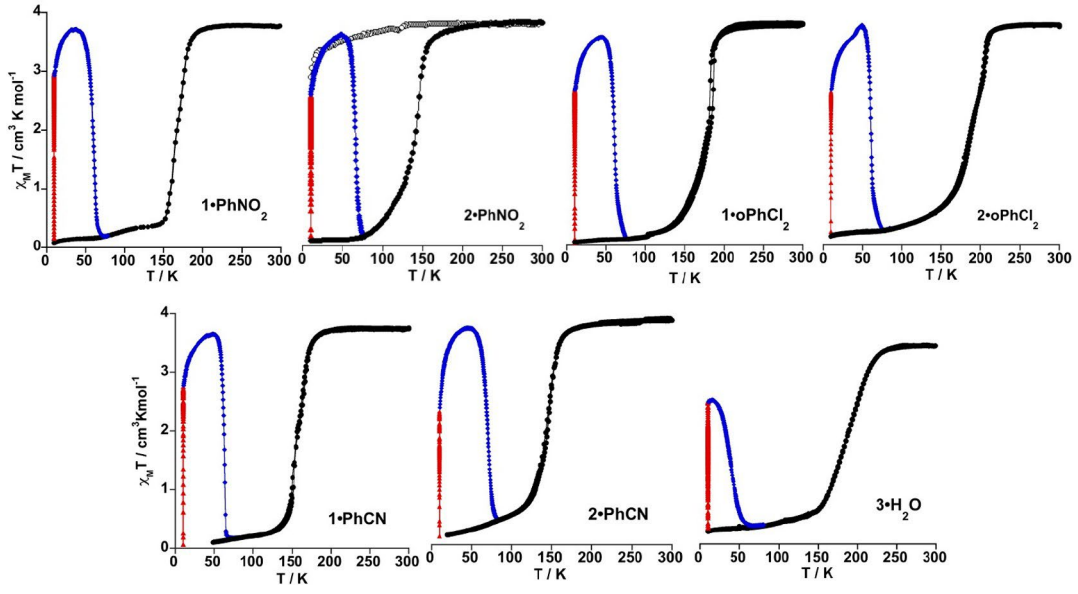

Figure 4. Magnetic and photomagnetic properties of 1·Guest, 2·Guest, and 3·H_2O: irradiation at 10 K (red triangles); thermal dependence of $\chi_M T$ upon heating at 0.3 K/min (blue circles) and heating/cooling at 1 K/min (black circles); thermal variation of $\chi_M T$ for crystals of 2·$PhNO_2$ soaked in mother liquor (open circles).

is generated through coordination of the N4 atom belonging to L^{N4}. Consequently, L^{N4} acts as a tetratopic ligand connecting the Fe^{II} and the Ag^{I} of the $[Ag_2(CN)_3]^-$ units, defining an irregular 2D grid with triangular and hexagonal windows. These layers are connected through the linear $[Ag(CN)_2]^-$ bridges, thus defining a quite open 3D framework. Alternatively, the structure can be described as constituted by an infinite stack of undulated $\{Fe_4[Ag(CN)_2]_2[Ag_2(CN)_3]_2\}_n$ layers pillared by L^{N4}. The space generated by the undulated rectangular windows allows interpenetration of two additional identical frameworks, thus filling the void space and affording a triple-interpenetrated system where there is only free room for one H_2O per formula unit (see Figure S6a). A simplified version of the structure showing the topology of the resulting (2-c)(3-c)2(4-c)(6-c) 4-nodal net analyzed with ToposPro[12] is given in Figure S6b.

Magnetic and Photomagnetic Properties. The thermal dependence of the $\chi_M T$ product (χ_M is the molar magnetic susceptibility and T is the temperature) was measured at 1 K min^{-1} using a magnetic field of 1 T in the temperature region 10−300 K for compounds 1·Guest, 2·Guest, and 3·H_2O. The corresponding $\chi_M T$ versus T curves are shown in Figure 4. At 300 K, the $\chi_M T$ value was found in the interval 3.70−3.76 cm^3 K mol^{-1} for 1·Guest and 2·Guest and 3.34 cm^3 K mol^{-1} for 3·H_2O. These values are typical for an $S = 2$ ground state with noticeable orbital contribution, as usually observed for the Fe^{II} ion in the HS state. For 1·Guest and 2·Guest, $\chi_M T$ is nearly constant in the temperature interval 300−210 K. Upon further cooling, $\chi_M T$ decreases abruptly, attaining values in the interval 0.10−0.25 cm^3 K mol^{-1} at 50 K, indicating that the LS state ($S = 0$) is practically fully populated. The equilibrium temperatures of the SCO, at which the molar fractions of the HS and the LS species are equal to $\gamma_{LS} = \gamma_{HS} = 0.5$ ($\Delta G_{HL} = 0$), have $T_{1/2}$ values equal to 156 K (1·PhCN), 145 K (2·PhCN), 166 K (1·$PhNO_2$), 143 K (2·$PhNO_2$), 180 K (1·o$PhCl_2$), and 187 K (2·o$PhCl_2$).

As mentioned in the structural analysis, an apparent inconsistency in the degree of spin-state conversion was found when the $\chi_M T$ product and the average Fe−N bond distance of 2·$PhNO_2$ at 120 K were correlated. This was associated with the clathration of a variable small amount of loosely attached methanol molecules, which spontaneously desorb at higher temperatures. To clarify this, the thermal variation of $\chi_M T$ was recorded for a crystalline sample of 2·$PhNO_2$ soaked in mother liquor. The results included in Figure 4 (open circles) demonstrates that under these conditions 2·$PhNO_2$ remains in the HS state at all temperatures.

Compound 3·H_2O experiments a similar SCO behavior starting at higher temperature (ca. 250 K), but the $\chi_M T$ product decreases more gradually. Indeed, the $\chi_M T$ value changes from 3.34 to 0.56 cm^3 K mol^{-1} ($\gamma_{HS} \approx 0.17$) in the temperature interval 250−150 K. Furthermore, a subsequent smoother decrease of $\chi_M T$ is observed in the temperature range 150−50 K, attaining a value of 0.26 cm^3 K mol^{-1} at 50 K ($\gamma_{HS} \approx 0.08$). The SCO can also be considered complete and characterized by a $T_{1/2}$ value of ca. 187 K.

Photogeneration of the metastable HS* state at low temperature, the so-called light-induced excited spin state trapping (LIESST) experiment,[13] was carried out at 10 K on irradiation of microcrystalline samples (0.80 mg) of 1·Guest and 2·Guest with red light (λ 633 nm), in the time required to attain saturation (Figure 4 and Figure S7). Under these conditions, the samples saturate in 3 h, with values of $\chi_M T$ in the interval 2.97−2.21 cm^3 K mol^{-1}. Subsequently, the light irradiation was switched off and the temperature increased at a rate of 0.3 K min^{-1}. Then, $\chi_M T$ keeps on increasing to reach a maximum of 3.72−3.54 cm^3 K mol^{-1} in the temperature interval 37−50 K. This increase in $\chi_M T$ corresponds to the thermal population of different microstates originating from the zero-field splitting of the $S = 2$ HS* spin state. At higher temperatures, $\chi_M T$ decreases rapidly until it joins the thermal SCO curve in the 65−84 K temperature range, indicating that the metastable HS* state has completely relaxed to the stable LS state. In contrast, after saturation $\chi_M T$ values experience just a slight increase to attain a maximum of ca. 2.47 cm^3 K

mol^{-1} at 14 K for 3·H_2O. This less stable HS* state relaxes back to the LS state at significantly lower temperatures. The characteristic T_{LIESST} temperatures,[14] obtained from $\partial\chi_M T/\partial T$ in the 10−77 K interval, are 63.6 K (1·PhCN), 70.5 K (2·PhCN), 61.0 K (1·$PhNO_2$), 66.0 K (2·$PhNO_2$), 60.5 K (1·o$PhCl_2$), 60.0 K (2·o$PhCl_2$), and 37 K (3·H_2O).

DISCUSSION

The objective of the present work was to investigate new cyanido-bridged bimetallic Fe^{II}-M^I SCO coordination polymers. We focused our attention on L^{N3} and L^{N4} tri- and tetratopic ligands, respectively. As mentioned above, it is relevant to stress that the isostructural doubly interpenetrated frameworks 1·Guest and 2·Guest could only be obtained in the presence of appropriate guest molecules such as $PhNO_2$, *o*-$PhCl_2$, and PhCN, which apparently act as templates during the self-assembly process. In addition, this template function was critically dependent on the size of the guest molecule.

Despite being L^{N3} being topologically identical with the ligand TPT, they form in combination with Fe^{II} and $[M^I(CN)_2]^-$ (M^I = Ag, Au) complexes with different stoichiometries and radically distinct $\{Fe[M^I(CN)_2]_2\}_n$ frameworks.[11] The complexes $\{Fe(TPT)_{2/3}[M^I(CN)_2]_2\}\cdot n$(Guest) ($M^I$ = Ag, Au) generate two interlocking 3D networks with an NbO-type topology defined by the $[N\square C-M^I-C\square N]^-$ linkers. The *c* axis of the network coincides with one of the diagonals of the NbO units, which in turn runs along the C_3 axis passing through the TPT ligands (see Figure 5). Indeed,

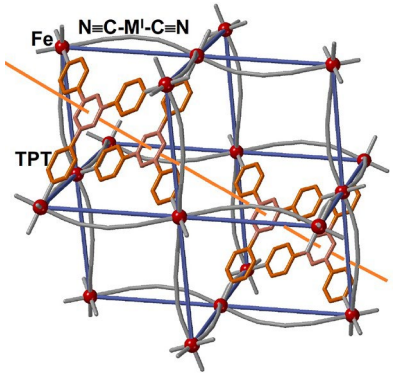

Figure 5. Fragment of the $\{Fe(TPT)_{2/3}[M^I(CN)_2]_2\}$ framework displaying the NbO-type topology defined by blue bars connecting the Fe^{II} centers (red spheres). The $[M^I(CN)_2]^-$ units are the undulating gray segments linking the Fe^{II} centers. The orange line denotes the diagonal and C_3 axis of the structure passing through the TPT ligands.

the TPT ligand is perfectly complementary with the voids generated by the pseudohexagonal circuits $\{Fe[M^I(CN)_2]\}_6$ (chair conformation) and acts as an additional tritopic bridge between the Fe^{II} centers. Obviously, extension of the linker between the pyridine and triazine moieties of the TPT ligand with alkaline spacers to afford a ligand having the same metrics as L^{N3} would provoke a severe misfit of the resulting ligand with respect to the size of the $\{Fe[M^I(CN)_2]\}_6$ circuits. As a consequence, the framework $\{Fe[M^I(CN)_2]_2\}_n$ cannot generate the intricate 3D NbO-type structure observed for the TPT system; in contrast, it readapts to form an infinite stack of 2D corrugated layered structures pillared by L^{N3} to afford 1·Guest and 2·Guest frameworks. Apparently, there is no stable structural arrangement compatible with L^{N3} acting as a tritopic ligand.

In contrast to L^{N3}, self-assembly of Fe^{II}, L^{N4}, and $[M^I(CN)_2]^-$ only gave positive results for M^I = Ag, affording 3·H_2O in low yield. During the slow diffusion process, part of the $[Ag^I(CN)_2]^-$ groups dissociate to generate in situ the relatively uncommon oligomeric species $[Ag^I_2(CN)_3]^-$, which has been described for a few related SCO compounds.[1] This fact together with the particular configuration of the pyridine rings in L^{N4} favors the expansion of the coordination number of the two equivalent Ag^I centers of $[Ag^I_2(CN)_3]^-$ to 3 (pseudotrigonal), thereby provoking strong distortion from linearity in this species and marked corrugation in the resulting 2D $\{Fe[Ag(CN)_2][Ag_2(CN)_3]\}_n$ layers. These layers stack along the [100] direction and are firmly attached to each other through L^{N4}, which act as double pillars linking two Fe^{II} and Ag^I (pseudotrigonal) pairs of adjacent layers, forming an open 3D framework. Furthermore, the wide rectangular $\{Fe_4[Ag(CN)_2]_2[Ag_2(CN)_3]_2\}$ windows facilitate interpenetration of two other identical frameworks in such a way that there is no room for inclusion of guest molecules. Indeed, only a loosely attached molecule of water is retained. The much more inert nature of the Au^I coordination sphere does not enable generating similar species, and consequently, the homologous gold compound of 3·H_2O cannot form.

As far as the SCO equilibrium temperatures ($T_{1/2}$) are concerned, a moderate increase in $T_{1/2}$ is observed for 1·Guest in the sequence PhCN (156 K) < $PhNO_2$ (166 K) < *o*-$PhCl_2$ (180 K). A possible explanation for this trend could be related to the slightly different sizes and shapes of these molecules. Their different accommodation requirements in the available space most likely favors distinct distributions of the intermolecular interactions which enhance the stabilization of the LS. This is also valid, to a first approximation, for 2·Guest (PhCN (145 K) ≈ $PhNO_2$ (143 K) < *o*-$PhCl_2$ (187 K)), although it is not obvious to explain why $T_{1/2}$ for the $PhNO_2$ derivative is virtually the same as that for the PhCN derivative. In this respect, it is well known the high sensitivity of $T_{1/2}$ to very small changes in free energy between of the HS and LS states, ΔG_{HL},[6c] is well-known, which in turn reflects the high sensitivity of the SCO centers to chemical pressure. Consequently, stabilization/destabilization of the LS (HS) state, and hence the value $T_{1/2}$, depends on a delicate balance between electronic and structural factors that often are difficult (if not impossible) to evaluate/discuss without a notable dose of speculation.

The general trend of the T_{LIESST} values is consistent with the empirical inverse-energy-gap law:[16] i.e., the metastability of the photogenerated HS* species decreases as the stability of the LS increases. This is particularly true for the $T_{1/2}$−T_{LIESST}[14] values of homologous pairs 1·Guest−2·Guest (Guest = PhCN, $PhNO_2$), although in the case of Guest = *o*-$PhCl_2$ the smaller difference in $T_{1/2}$ is reflected in virtually similar T_{LIESST} values (the same can be observed when 2·PhCN and 2·$PhNO_2$ are compared). It is important to remark that all the $T_{1/2}$−T_{LIESST} pairs in the 1·Guest−2·Guest series are located close to the correlation line $T_{LIESST} = T_0 - 0.3T_{1/2}$, with T_0 = 100 K being typical for less rigid coordination centers $[Fe^{II}N_6]$ constituted of monodentate ligands and being consistent with their isostructural nature.[14] In contrast, despite the fact that $[Fe^{II}N_6]$ centers are similar for 3·H_2O, its corresponding $T_{1/2}$−T_{LIESST} pair is well below this line. This may reflect the distinct structural nature of the latter, which displays a densely

packed triply interpenetrated 3D rigid structure versus a less densely packed and probably less rigid doubly interpenetrated 3D structure in 1·Guest and 2·Guest.

It is a general fact when series of isostructural Ag^I and Au^I SCO complexes are compared that $(T_{1/2})^{Ag} > (T_{1/2})^{Au}$. This is usually rationalized in terms of lower donor ability associated with the greater electron-withdrawing ability of the cyanide group due to a more covalent NC−Au interaction. This general trend applies for the isostructural 1·Guest and 2·Guest compounds when Guest is $PhNO_2$ and PhCN, but it does not apply for *o*-$PhCl_2$. In line with what is mentioned above, the presumed extra space required by *o*-$PhCl_2$ together with the more rigid nature of the Au framework, in comparison with the Ag^I framework, may favor an extra chemical pressure which results in a higher than expected $T_{1/2}$ value. This conjecture is supported by the greater number of short intermolecular contacts observed for 2·$PhNO_2$ in comparison with 1·$PhNO_2$.

CONCLUSION

Two new ligands with unusual coordination denticities, trigonal (L^{N3}) and square (L^{N4}), have been included in the library of SCO Hofmann-type metal−organic frameworks derived from $[M^I(CN)_2]^-$ (M^I = Ag, Au). Using slow diffusion methods in presence of appropriate guest molecules, L^{N3} affords six new isostructural clathrate compounds generically formulated as 1·Guest and 2·Guest with Guest = PhCN, $PhNO_2$, *o*-$PhCl_2$. The structure of the $PhNO_2$ derivative shows that L^{N3} works as a bis-monodentate ligand to satisfy, most likely, the metrics imposed by the $\{Fe[M^I(CN)_2]_2\}_n$ layers, thereby acting as a pillar between the layers, thus affording an open 3D framework. Two identical frameworks interpenetrate in the same space and hold together through short intermolecular interactions including weak $M^I\cdots M^I$ metallophilic interactions. The six clathrates exhibit thermal- and light-induced SCO properties. Concerning the ligand L^{N4}, one should expect coordination of four Fe^{II} and generation of a complicated framework via $[M^I(CN)_2]^-$; however, the occurrence of geometric incompatibilities is apparent, which are solved for the Ag^I derivative by virtue of its much more labile coordination sphere. Consequently, the structure of 3·H_2O is made up of extended $\{Fe[Ag^I(CN)_2][Ag_2^I(CN)_3]\}_n$ layers pillared by two opposite pyridine rings of L^{N4}, which act as axial ligands of Fe^{II}, while the remaining two pyridine rings coordinate the Ag^I centers of the in situ generated $[Ag_2^I(CN)_3]^-$ units. The much more inert nature of Au^I prevents the formation of this uncommon triple-interpenetrated network. The higher characteristic $T_{1/2}$ value of the SCO is consistent with the incomplete photogeneration of the LS state at low temperatures.

EXPERIMENTAL SECTION

Materials. $Fe(BF_4)_2\cdot 6H_2O$, $K[Ag(CN)_2]$, $K[Au(CN)_2]$, and organic precursors were purchased from commercial sources and used as received.

Synthesis of Ligands. 4-Ethynylpyridine and the ligands L^{N3} and L^{N4} were prepared by the published methods.[17]

Synthesis of $\{Fe^{II}(L^{N3})[M^I(CN)_2]_2\}$·Guest ($M^I$ = Ag (1·Guest), Au (2·Guest)). Crystals of 1·Guest and 2·Guest were obtained in the same manner by slow diffusion of methanolic solutions of four reagents placed in a modified H-shaped vessel with four arms. Each reagent was deposited in one of the arms, in the following order: $Fe(BF_4)_2\cdot 6H_2O$ (0.0787 mmol, 26.6 mg), L^{N3} (0.0787 mmol, 30 mg), Guest (=$PhNO_2$, PhCN, *o*-$PhCl_2$; 2 mL, large excess), and $K[Ag(CN)_2]$ (0.1574 mmol, 31.5 mg) (1)/$K[Au(CN)_2]$ (0.1574 mmol, 47.3 mg) (2). Finally, the vessel was filled completely with methanol and sealed. In all cases, yellow crystals appeared within 2 weeks, in low yield (ca. 20%). EDX analysis (energy dispersive X-ray analysis) confirmed the stoichiometric relationship between metallic coordination centers: for 1·Guest, Fe:Ag = 1:2; for 2·Guest, Fe:Au = 1:2.

Complex 1·Guest. Anal. Calcd for $C_{37}H_{20}Ag_2FeN_8O_2$ (880.20): C, 50.49; H, 2.29; N, 12.73. Found: C, 50.38; H, 2.32; N, 12.58. Calcd for $C_{37}H_{19}Ag_2FeN_7Cl_2$ (904.09): C, 49.16; H, 2.12; N, 10.85. Found: C, 50.18; H, 2.22; N, 10.98. Calcd for $C_{38}H_{20}Ag_2FeN_8$ (860.22): C, 53.06; H, 2.34; N, 13.03. Found: C, 52.58; H, 2.32; N, 12.68. IR (cm^{-1}): ν(C≡C) 2219 (m), ν(C≡N) 2163 (s), ν(C≡N) 1613 (vs), ν(pyridine ring) 1418 (s), 825 (s). The symmetric and asymmetric stretching modes of the NO_2 group in $PhNO_2$ were unambiguously assigned to $\nu_a(NO_2)$ 1525 (vs) and $\nu_s(NO_2)$ 1344 (vs). No singular signals could be associated with PhCN and *o*-$PhCl_2$.

Complex 2·Guest. Anal. Calcd for $C_{37}H_{20}Au_2FeN_8O_2$ (1058.39): C, 41.99; H, 1.90; N, 10.59. Found: C, 41.78; H, 1.98; N, 10.43. Calcd for $C_{37}H_{19}Au_2FeN_7Cl_2$ (1082.29): C, 41.06; H, 1.77; N, 9.06. Found: C, 42.03; H, 1.85; N, 10.43. Calcd for $C_{38}H_{20}Au_2FeN_8$ (1038.41): C, 43.95; H, 1.94; N, 10.79. Found: C, 43.58; H, 2.01; N, 10.68. IR (cm^{-1}): ν(C≡C) 2220 (m), ν(C≡N) 2170 (s), ν(C≡N) 1610 (vs), ν(pyridine ring) 1420 (s), 820 (s). The symmetric and asymmetric stretching modes of the NO_2 group in $PhNO_2$ were unambiguously assigned to $\nu_a(NO_2)$ 1520 (vs) and $\nu_s(NO_2)$ 1340 (vs). No singular signals could be associated with *o*-$PhCl_2$ and PhCN.

Synthesis of $\{Fe^{II}(L^{N4})[Ag_2(CN)_3][Ag(CN)_2]\}\cdot H_2O$ ($3\cdot H_2O$). Crystals of $3\cdot H_2O$ were obtained by slow diffusion of solutions of three reagents placed in a modified H-shaped vessel with three arms, the arm in the middle being broader than the peripheral arms. This feature was introduced due to the high insolubility of L^{N4} (a high volume of solvent was needed to dissolve the appropriated amount of ligand). The peripheral vessel arms contained $Fe(BF_4)_2\cdot 6H_2O$ (0.05925 mmol, 20 mg) and $K[Ag(CN)_2]$ (0.1185 mmol, 23.7 mg), respectively; the central vessel arm contained a solution of L^{N4} (0.05925 mmol, 28.6 mg, dissolved in 7 mL of $CHCl_3$). Finally, the tube was filled completely with methanol and sealed. Orange single crystals of $3\cdot H_2O$ appeared within 4 weeks, in low yield (ca. 20%).

EDX analysis (energy dispersive X-ray analysis) confirmed the stoichiometric relationship between metallic coordination centers: for $3\cdot H_2O$, Fe:Ag = 1:3.

Complex $3\cdot H_2O$. Anal. Calcd for $C_{39}H_{20}Ag_3FeN_9O$ (1010.10): C, 46.37; H, 2.00; N, 12.48. Found: C, 46.59; H, 2.10; N, 12.73. IR (cm^{-1}): ν(C≡C) 2212 (w), ν(C≡N) 2150 (m), ν(C≡N) 1604 (vs), ν(pyridine rings) 1419 (s), 813 (s).

Physical Characterization. Variable-temperature magnetic susceptibility measurements were performed on samples (20−30 mg) consisting of crystals, using a Quantum Design MPMS2 SQUID susceptometer equipped with a 5.5 T magnet, operating at 1 T and at temperatures in the range 300−1.8 K. Experimental susceptibilities were corrected for diamagnetism of the constituent atoms by the use of Pascal's constants. Thermogravimetric analysis was performed on a Mettler Toledo TGA/SDTA 851e instrument in the 290−800 K temperature range under a nitrogen atmosphere with a rate of 10 K min^{-1}.

Single-Crystal X-ray Diffraction. Single-crystal X-ray data were collected with an Oxford Diffraction Supernova diffractometer. In all cases, Mo Kα radiation (λ = 0.71073 Å) was used. Data scaling and empirical or multiscan absorption corrections were performed. The structures were solved by direct methods with SHELXT or SIR2004 and refined by full-matrix least-squares techniques on F^2 with SHELXL.[18] Non-hydrogen atoms were refined anisotropically, and hydrogen atoms were placed in calculated positions and refined in idealized geometries (riding model) with fixed isotropic displacement parameters.

ASSOCIATED CONTENT

AUTHOR INFORMATION

Corresponding Author

*E-mail for J.A.R.: jose.a.real@uv.es.

ORCID

José A. Real: 0000-0002-2302-561X

Notes

The authors declare no competing financial interest.

ACKNOWLEDGMENTS

We thank the Spanish Ministerio de Economía y Competitividad (MINECO) and FEDER funds (CTQ2013-46275-P and CTQ2016-78341-P and Unidad de Excelencia María de Maeztu MDM-2015-0538), and Generalitat Valenciana (PROMETEO/2016/147). F.J.V.-M. thanks MINECO for a predoctoral FPI grant. We also thank Dr. Carlos Martí for helping us with ToposPro software.

REFERENCES

(1) See for example: (a) Hauser, A. Intersystem Crossing in Iron(II) Coordination Compounds: A Model Process between Classical and Quantum Mechanical Behaviour. *Comments Inorg. Chem.* 1995, *17*, 17−40. (b) König, E. Nature and Dynamics of the Spin-State Interconversion in Metal-Complexes. *Struct. Bonding (Berlin, Ger.)* 1991, *76*, 51−152. (c) Gütlich, P.; Hauser, A.; Spiering, H. Thermal and Optical Switching of Iron(II) Complexes. *Angew. Chem., Int. Ed. Engl.* 1994, *33*, 2024−2054. (d) Sato, O. Optically Switchable Molecular Solids: Photoinduced Spin-Crossover, Photochromism, and Photoinduced Magnetization. *Acc. Chem. Res.* 2003, *36*, 692−700. (e) Real, J. A.; Gaspar, A. B.; Niel, V.; Muñoz, M. C. Communication between Iron(II) Building Blocks in Cooperative Spin Transition Phenomena. *Coord. Chem. Rev.* 2003, *236*, 121−141. (f) Spin Crossover in Transition Metal Compounds I-III. *Topics in Current Chemistry*; Gütlich, P., Goodwin, H. A., Eds.; Springer: 2004, Vols. *233*−*235*. (g) Real, J. A.; Gaspar, A. B.; Muñoz, M. C. Thermal, Pressure and Light Switchable Spin-Crossover Materials. *Dalton Trans.* 2005, 2062−2079. (h) Halcrow, M. A. The Spin-States and Spin-Transitions of Mononuclear Iron(II) Complexes of Nitrogen-Donor Ligands. *Polyhedron* 2007, *26*, 3523−3576. (i) Halcrow, M. A. Iron(II) Complexes of 2,6-di(pyrazol-1-yl)pyridines A Versatile System for Spin-Crossover Research. *Coord. Chem. Rev.* 2009, *253*, 2493−2514. (j) Olguin, J.; Brooker, S. Spin Crossover Active Iron(II) Complexes of Selected pyrazole-pyridine/pyrazine Ligands. *Coord. Chem. Rev.* 2011, *255*, 203−240. (k) Bousseksou, A.; Molnár, G.; Salmon, L.; Nicolazzi, W. Molecular Spin Crossover Phenomenon: Recent Achievements and Prospects. *Chem. Soc. Rev.* 2011, *40*, 3313−3335.

(2) (a) Meded, V.; Bagrets, A.; Fink, K.; Chandrasekar, R.; Ruben, M.; Evers, F.; Bernand-Mantel, A.; Seldenthuis, J. S.; Beukman, A.; van der Zant, H. S. J. Electrical Control over the Fe(II) Spin Crossover in a Single Molecule: Theory and Experiment. *Phys. Rev. B: Condens. Matter Mater. Phys.* 2011, *83*, 245415. (b) Prins, F.; Monrabal-Capilla, M.; Osorio, E. A.; Coronado, E.; van der Zant, H. S. J. Room-Temperature Electrical Addressing of a Bistable Spin-Crossover Molecular System. *Adv. Mater.* 2011, *23*, 1545−1549. (c) Cavallini, M.; Bergenti, I.; Milita, S.; Kengne, J. C.; Gentili, D.; Ruani, G.; Salitros, I.; Meded, V.; Ruben, M. Thin Deposits and Patterning of Room-Temperature-Switchable One-Dimensional Spin-Crossover Compounds. *Langmuir* 2011, *27*, 4076−4081. (d) Miyamachi, T.; Gruber, M.; Davesne, V.; Bowen, M.; Boukari, S.; Joly, L.; Scheurer, F.; Rogez, G.; Yamada, T. K.; Ohresser, P.; Beaurepaire, E.; Wulfhekel, W. Robust Spin Crossover and Memristance across a Single Molecule. *Nat. Commun.* 2012, *3*, 938. (e) Martinho, P. N.; Rajnak, C.; Ruben, M. In *Spin-Crossover Materials: Properties and Applications*; Halcrow, M. A., Ed.; Wiley: 2013; pp 376−404 and references therein. (f) Shepherd, H. J.; Molnár, G.; Nicolazzi, W.; Salmon, L.; Bousseksou, A. Spin Crossover at the Nanometre Scale. *Eur. J. Inorg. Chem.* 2013, *2013*, 653−661. (g) Rotaru, A.; Dugay, J.; Tan, R. P.; Gural'skiy, I. A.; Salmon, L.; Demont, P.; Carrey, J.; Molnár, G.; Respaud, M.; Bousseksou, A. Nano-Electromanipulation of Spin Crossover Nanorods: Towards Switchable Nanoelectronic Devices. *Adv. Mater.* 2013, *25*, 1745−1749. (h) Gural'skiy, I. A.; Quintero, C. M.; Sánchez Costa, J.; Demont, P.; Molnár, G.; Salmon, L.; Shepherd, H. J.; Bousseksou, A. Spin Crossover Composite Materials for Electrothermomechanical Actuators. *J. Mater. Chem. C* 2014, *2*, 2949−2955. (i) Bartual-Murgui, C.; Akou, A.; Thibault, C.; Molnár, G.; Vieu, C.; Salmon, L.; Bousseksou, A. Spin-Crossover Metal-Organic Frameworks: Promising Materials for Designing Gas Sensors. *J. Mater. Chem. C* 2015, *3*, 1277−1285. (j) Aragonés, A. C.; Aravena, D.; Cerdá, J. I.; Acís-Castillo, Z.; Li, H.; Real, J. A.; Sanz, F.; Hihath, J.; Ruiz, E.; Díez-Pérez, I. Large Conductance Switching in a Single-Molecule Device through Room Temperature Spin-Dependent Transport. *Nano Lett.* 2016, *16*, 218−226.

(3) (a) Muñoz, M. C.; Real, J. A. Thermo-, Piezo-, Photo- and Chemo-Switchable Spin Crossover Iron(II)-Metallocyanate Based Coordination Polymers. *Coord. Chem. Rev.* 2011, *255*, 2068−2093. (b) Muñoz, M. C.; Real, J. A. Polymeric Spin-Crossover Materials. In *Spin-Crossover Materials: Properties and Applications*; Halcrow, M. A., Ed.; Wiley: 2013; pp 121−146. (c) Ni, Z.-P.; Liu, J.-L.; Hoque, Md. N.; Liu, W.; Li, J.-Y.; Chen, Y.-C.; Tong, M.-L. Recent advances in guest effects on spin-crossover behavior in Hofmann-type metal-organic frameworks. *Coord. Chem. Rev.* 2017, *335*, 28−43.

(4) (a) Martínez, V.; Gaspar, A. B.; Muñoz, M. C.; Bukin, G. V.; Levchenko, G.; Real, J. A. Synthesis and Characterisation of a New Series of Bistable Iron (II) Spin-Crossover 2D Metal-Organic Frameworks. *Chem. - Eur. J.* 2009, *15*, 10960−10971. (b) Ohtani, R.; Arai, M.; Ohba, H.; Hori, A.; Takata, M.; Kitagawa, S.; Ohba, M. Modulation of the Interlayer Structures and Magnetic Behaviour of 2D Spin-Crossover Coordination Polymers $[Fe^{II}(L)_2Pt^{II}(CN)_4]$. *Eur. J. Inorg. Chem.* 2013, *2013*, 738−744. (c) Klein, Y. M.; Sciortino, N. F.; Ragon, F.; Housecroft, C. E.; Kepert, C. J.; Neville, S. M. Spin crossover intermediate plateau stabilization in a flexible 2-D Hofmann-type coordination polymer. *Chem. Commun.* 2014, *50*, 3838−3840. (d) Liu, W.; Wang, L.; Su, Y.-J.; Chen, Y.-C.; Tucek, J.; Zboril, R.; Ni, Z.-P.; Tong, M.-L. Hysteretic Spin Crossover in Two-Dimensional (2D) Hofmann-Type Coordination Polymers. *Inorg. Chem.* 2015, *54*, 8711−8716. (e) Milin, E.; Patinec, V.; Triki, S.; Bendeif, E.-E.; Pillet, S.; Marchivie, M.; Chastanet, G.; Boukheddaden, K. Elastic Frustration Triggering Photoinduced Hidden Hysteresis and Multistability in a Two-Dimensional Photoswitchable Hofmann-Like Spin-Crossover Metal-Organic Framework. *Inorg. Chem.* 2016, *55*, 11652−11661. (f) Valverde-Muñoz, F. J.; Seredyuk, M.; Muñoz, M. C.; Znovjyak, K.; Fritsky, I. O.; Real, J. A. Strong Cooperative Spin

Crossover in 2D and 3D Fe^{II}-$M^{I,II}$ Hofmann-Like Coordination Polymers Based on 2-Fluoropyrazine. *Inorg. Chem.* 2016, *55*, 10654−10665. (g) Kucheriv, O. I.; Shylin, S. I.; Ksenofontov, V.; Dechert, S.; Haukka, M.; Fritsky, I. O.; Gural′skiy, I. A. Spin Crossover in Fe(II)-M(II) Cyanoheterobimetallic Frameworks (M = Ni, Pd, Pt) with 2-Substituted Pyrazines. *Inorg. Chem.* 2016, *55*, 4906−4914. (h) Sciortino, N. F.; Zenere, K. A.; Corrigan, M. E.; Halder, G. J.; Chastanet, G.; Letard, J.-F.; Kepert, C. J.; Neville, S. M. Four-step iron (II) spin state cascade driven by antagonistic solid state interactions. *Chem. Sci.* 2017, *8*, 701−707. (i) Liu, F.-L.; Tao, J. Hysteretic Two-Step Spin-Crossover Behaviour in Two Two-Dimensional Hofmann-Type Coordination Polymers. *Chem. - Eur. J.* 2017, *23*, 18252−18257.

(5) (a) Niel, V.; Martinez-Agudo, J. M.; Muñoz, M. C.; Gaspar, A. B.; Real, J. A. Cooperative Spin Crossover Behaviour in Cyanide-Bridged Fe(II)-M(II) Bimetallic 3D Hofmann-like Networks (M = Ni, Pd, Pt). *Inorg. Chem.* 2001, *40*, 3838−3839. (b) Agustí, G.; Cobo, S.; Gaspar, A. B.; Molnar, G.; Moussa, N. O.; Szilagyi, P. A.; Palfi, V.; Vieu, C.; Muñoz, M. C.; Real, J. A.; Bousseksou, A. Thermal and Light-Induced Spin Crossover Phenomena in New 3D Hofmann-Like Microporous Metalorganic Frameworks Produced As Bulk Materials and Nanopatterned Thin Films. *Chem. Mater.* 2008, *20*, 6721−6732. (c) Bartual-Murgui, C.; Ortega-Villar, N. A.; Shepherd, H. J.; Muñoz, M. C.; Salmon, L.; Molnar, G.; Bousseksou, A.; Real, J. A. Enhaced porosity in a new 3D Hofmann-like network exhibiting humidity sensitive cooperative spin transitions at room temperature. *J. Mater. Chem.* 2011, *21*, 7217−7222. (d) Sciortino, N. F.; Scherl-Gruenwald, K. R.; Chastanet, G.; Hader, G. J.; Chapman, K. W.; Letard, J.-F.; Kepert, C. J. Hysteretic Three-Step Spin Crossover in a Thermo- and Photochromic 3D Pillared Hofmann-type Metal-Organic Framework. *Angew. Chem.* 2012, *124*, 10301−10305. (e) Muñoz-Lara, F. J.; Gaspar, A. B.; Muñoz, M. C.; Ksenofontov, V.; Real, J. A. Novel Iron(II) Microporous Spin-Crossover Coordination Polymers with Enhaced Pore Size. *Inorg. Chem.* 2013, *52*, 3−5. (f) Muñoz-Lara, F. J.; Gaspar, A. B.; Muñoz, M. C.; Arai, M.; Kitagawa, S.; Ohba, M.; Real, J. A. Sequestering Aromatic Molecules with a Spin-Crossover Fe^{II} Microporous Coordination Polymer. *Chem. - Eur. J.* 2012, *18*, 8013−8018. (g) Piñeiro-Lopez, L.; Seredyuk, M.; Muñoz, M. C.; Real, J. A. Two- and one-step cooperative spin transitions in Hofmann-like clathrates with enhanced loading capacity. *Chem. Commun.* 2014, *50*, 1833−1835. (h) Piñeiro-Lopez, L.; Valverde-Muñoz, F. J.; Seredyuk, M.; Muñoz, M. C.; Haukka, M.; Real, J. A. Guest Induced Strong Cooperative One- and Two-Step Spin Transitions in Highly Porous Iron(II) Hofmann-Type Metal-Organic Frameworks. *Inorg. Chem.* 2017, *56*, 7038−7047. (i) Bao, X.; Shepherd, H. J.; Salmon, L.; Molnar, G.; Tong, M. L.; Bousseksou, A. The Effect of an Active Guest on the Spin Crossover Phenomenon. *Angew. Chem., Int. Ed.* 2013, *52*, 1198−1202. (j) Liu, W.; Peng, Y. Y.; Wu, S. G.; Chen, Y. C.; Hoque, M. N.; Ni, Z. P.; Chen, X. M.; Tong, M. L. Guest-Switchable Multi-Step Spin Transitions in an Amine-Functionalized Metal-Organic Framework. *Angew. Chem., Int. Ed.* 2017, *56*, 14982−14986.

(6) (a) Bartual-Murgui, C.; Salmon, L.; Akou, A.; Ortega-Villar, N. A.; Shepherd, H. J.; Muñoz, M. C.; Molnar, G.; Real, J. A.; Bousseksou, A. Synergetic Effect of Host-Guest Chemistry and Spin Crossover in 3D Hofmann-like Metal-Organic Frameworks [Fe(bpac)M(CN)$_4$] (M = Pt, Pd, Ni). *Chem. - Eur. J.* 2012, *18*, 507−516. (b) Muñoz-Lara, F. J.; Gaspar, A. B.; Aravena, D.; Ruiz, E.; Muñoz, M. C.; Ohba, M.; Ohtani, R.; Kitagawa, S.; Real, J. A. Enhanced bistability by guest inclusion in Fe(II) spin crossover porous coordination polymers. *Chem. Commun.* 2012, *48*, 4686−4688. (c) Bartual-Murgui, C.; Amal, A.; Shepherd, H. J.; Molnar, G.; Real, J. A.; Salmon, L.; Bousseksou, A. Tunable Spin-Crossover Behavior of the Hofmann-like Network {Fe(bpac)[Pt(CN)$_4$]} through Host-Guest Chemistry. *Chem. - Eur. J.* 2013, *19*, 15036−15043. (d) Arcís-Castillo, Z.; Muñoz-Lara, F. J.; Muñoz, M. C.; Aravena, D.; Gaspar, A. B.; Sanchez-Royo, J. F.; Ruiz, E.; Ohba, M.; Matsuda, R.; Kitagawa, S.; Real, J. A. Reversible Chemisorption of Sulfur Dioxide in a Spin Crossover Porous Coordination Polymer. *Inorg. Chem.* 2013, *52*, 12777−12783. (e) Aravena, D.; Arcís-Castillo, Z.; Muñoz, M. C.; Gaspar, A. B.; Yoneda, K.; Ohtani, R.; Mishima, A.; Kitagawa, S.; Ohba, M.; Real, J. A.; Ruiz, E. Guest Modulation of Spin-Crossover Transition Temperature in a Porous Iron(II) Metal-Organic Framework: Experimental and Periodic DFT Studies. *Chem. - Eur. J.* 2014, *20*, 12864−12873.

(7) (a) Niel, V.; Thompson, A. L.; Muñoz, M. C.; Galet, A.; Goeta, A. E.; Real, J. A. Crystalline-State Reaction with Allosteric Effect in Spin-Crossover, Interpenetrated Networks with Magnetic and Optical Bistability. *Angew. Chem., Int. Ed.* 2003, *42*, 3760−3763. (b) Galet, A.; Niel, V.; Muñoz, M. C.; Real, J. A. Synergy between Spin Crossover and Metallophilicity in Triple Interpenetrated 3D Nets with the NbO Structure Type. *J. Am. Chem. Soc.* 2003, *125*, 14224−14225. (c) Galet, A.; Muñoz, M. C.; Martínez, V.; Real, J. A. Supramolecular isomerism in spin crossover networks with aurophilic interactions. *Chem. Commun.* 2004, 2268−2269.

(8) (a) Galet, A.; Gaspar, A. B.; Muñoz, M. C.; Bukin, G. V.; Levchenko, G.; Real, J. A. Tunable Bistability in a Three-Dimensional Spin-Crossover Sensory- and Memory-Functional Material. *Adv. Mater.* 2005, *17*, 2949−2953. (b) Ohba, M.; Yoneda, K.; Agustí, G.; Muñoz, M. C.; Gaspar, A. B.; Real, J. A.; Yamasaki, M.; Ando, H.; Nakao, Y.; Sakaki, S.; Kitagawa, S. Bidirectional Chemo-Switching of Spin State in a Microporous Framework. *Angew. Chem., Int. Ed.* 2009, *48*, 4767−4771. (c) Murphy, M. J.; Zenere, K. A.; Ragon, F.; Southon, P. D.; Kepert, C. J.; Neville, S. M. Guest Programmable Multistep Spin Crossover in a Porous 2-D Hofmann-Type Material. *J. Am. Chem. Soc.* 2017, *139*, 1330−1335. (d) Clements, J. E.; Price, J. R.; Neville, S. M.; Kepert, C. J. Perturbation of Spin Crossover Behavior by Covalent Post-Synthetic Modification of a Porous Metal−Organic Framework. *Angew. Chem., Int. Ed.* 2014, *53*, 10164−10168. (e) Li, J.-Y.; Chen, Y.-C.; Zhang, Z.-M.; Liu, W.; Ni, Z.-P.; Tong, M.-L. Tuning the Spin-Crossover Behaviour of a Hydrogen-Accepting Porous Coordination Polymer by Hydrogen-Donating Guests. *Chem. - Eur. J.* 2015, *21*, 1645−1651.

(9) (a) Cobo, S.; Molnar, G.; Real, J. A.; Bousseksou, A. Multilayer Sequential Assembly of Thin Films That Display Room-Temperature Spin Crossover with Hysteresis. *Angew. Chem., Int. Ed.* 2006, *45*, 5786−5789. (b) Molnar, G.; Cobo, S.; Real, J. A.; Carcenac, F.; Daran, E.; Vieu, C.; Bousseksou, A. A Combined Top-Down/Bottom-Up Approach for the Nanoscale Patterning of Spin-Crossover Coordination Polymers. *Adv. Mater.* 2007, *19*, 2163−2167. (c) Volatron, F.; Catala, L.; Rivière, E.; Gloter, A.; Stephan, O.; Mallah, T. Spin-Crossover Coordination Nanoparticles. *Inorg. Chem.* 2008, *47*, 6584−6586. (d) Boldog, I.; Gaspar, A. B.; Martínez, V.; Pardo-Ibañez, P.; Ksenofontov, V.; Bhattacharjee, A.; Gütlich, P.; Real, J. A. Spin-Crossover Nanocrystals with Magnetic, Optical, and Structural Bistability Near Room Temperature. *Angew. Chem., Int. Ed.* 2008, *47*, 6433−6437. (e) Martínez, V.; Boldog, I.; Gaspar, A. B.; Ksenofontov, V.; Bhattacharjee, A.; Gütlich, P.; Real, J. A. Spin Crossover Phenomenon in Nanocrystals and Nanoparticles of [Fe(3-Fpy)$_2$M(CN)$_4$] (M^{II}= Ni, Pd, Pt) Two-Dimensional Coordination Polymers. *Chem. Mater.* 2010, *22*, 4271−4281. (f) Bartual-Murgui, C.; Akou, A.; Salmon, L.; Molnar, G.; Thibault, C.; Real, J. A.; Bousseksou, A. Guest Effect on Nanopatterned Spin-Crossover Thin Films. *Small* 2011, *7*, 3385−3391. (g) Bartual-Murgui, C.; Akou, A.; Thibault, C.; Molnar, G.; Vieu, C.; Salmon, L.; Bousseksou, A. Spin-crossover metal-organic frameworks: promising materials for designing gas sensors. *J. Mater. Chem. C* 2015, *3*, 1277−1285.

(10) Shepherd, H. J.; Gural′skiy, I. A.; Quintero, C. M.; Tricard, S.; Salmon, L.; Molnar, G.; Bousseksou, A. Molecular actuators driven by cooperative spin-state switching. *Nat. Commun.* 2013, *4*, 2607.

(11) (a) Arcís-Castillo, Z.; Muñoz, M. C.; Molnar, G.; Bousseksou, A.; Real, J. A. [Fe(TPT)$_{2/3}${M^I(CN)$_2$}$_2$]·nSolv (M^I = Ag, Au), New Bimetallic Porous Coordination Polymers with Spin-Crossover Properties. *Chem. - Eur. J.* 2013, *19*, 6851−6861. (b) Piñeiro-Lopez, L.; Arcís-Castillo, Z.; Muñoz, M. C.; Real, J. A. Clathration of Five − Membered Aromatic Rings in the Bimetallic Spin Crossover Metal-Organic Framework [Fe(TPT)$_{2/3}${M^I(CN)$_2$}$_2$]·G (M^I = Ag, Au). *Cryst. Growth Des.* 2014, *14*, 6311−6319.

(12) Blatov, V. A.; Shevchenko, A. P.; Proserpio, D. M. Applied topological analysis of crystal structures with the program package ToposPro. *Cryst. Growth Des.* 2014, *14*, 3576−3586.

(13) (a) Decurtins, S.; Gütlich, P.; Köhler, P. C.; Spiering, H.; Hauser, A. Light-induced excited spin state trapping in a transition-metal complex: The hexa-1-propyltetrazole-iron(II) tetrafluoroborate spin-crossover system. *Chem. Phys. Lett.* 1984, *105*, 1−4. (b) Hauser, A. Reversibility of light-induced excited spin state trapping in the $Fe(ptz)_6(BF_4)_2$, and the $Zn_{1-x}Fe_x(ptz)_6(BF_4)_2$ spin-crossover systems. *Chem. Phys. Lett.* 1986, *124*, 543−548.

(14) (a) Létard, J. F.; Guionneau, P.; Rabardel, L.; Howard, J. A. K.; Goeta, A. E.; Chasseau, D.; Kahn, O. Structural, magnetic, and photomagnetic studies of a mononuclear iron(II) derivative exhibiting an exceptionally abrupt spin transition. Light-induced thermal hysteresis phenomenon. *Inorg. Chem.* 1998, *37*, 4432−4441. (b) Létard, J. F; Chastanet, G.; Guionneau, P. Optimizing the stability of trapped metastable spin states. In *Spin-Crossover Materials: Properties and Applications*; Halcrow, M. A. Ed.; Wiley: 2013; pp 475−500.

(15) (a) Niel, V.; Thompson, A. L.; Goeta, A. E.; Enachescu, C.; Hauser, A.; Galet, A.; Muñoz, M. C.; Real, J. A. Thermal- and photoinduced spin-state switching in an unprecedented three-dimensional bimetallic coordination polymer. *Chem. - Eur. J.* 2005, *11*, 2047−2060. (b) Kosone, T.; Suzuki, Y.; Ono, S.; Kanadani, C.; Saito, T.; Kitazawa, T. A new spin crossover heterometallic Fe(II)Ag(I) coordination polymer with the $[Ag_2(CN)_3]^-$ unit: crystallographic and magnetic study. *Dalton Trans.* 2010, *39*, 1786−1790. (c) Li, J.-Y.; Yan, Z.; Ni, Z.-P.; Zhang, Z.-M.; Chen, Y.-C.; Liu, W.; Tong, M.-L. Guest-effected spin-crossover in a novel three-dimensional self-penetrating coordination polymer with permanent porosity. *Inorg. Chem.* 2014, *53*, 4039−4046. (d) Piñeiro-López, L.; Valverde-Muñoz, F. J.; Seredyuk, M.; Bartual-Murgui, C.; Muñoz, M. C.; Real, J. A. Cyanido bridged Fe^{II}-M^{I} bimetallic Hofmann-like spin-crossover coordination polymers based on 2,6-Naphthyridine. *Eur. J. Inorg. Chem.* 2018, *2018*, 289−296.

(16) (a) Hauser, A. Intersystem crossing in Fe(II) coordination compounds. *Coord. Chem. Rev.* 1991, *111*, 275−290. (b) Hauser, A.; Vef, A.; Adler, P. Intersystem crossing dynamics in Fe(II) coordination compounds. *J. Chem. Phys.* 1991, *95*, 8710−8717. (c) Hauser, A.; Enachescu, C.; Daku, M. L.; Vargas, A.; Amstutz, N. Low-temperature lifetimes of metastable high-spin states in spin-crossover and in low-spin iron(II) compounds: the rule and exceptions to the rule. *Coord. Chem. Rev.* 2006, *250*, 1642−1652.

(17) (a) Ciana, L. D.; Haim, A. J. Synthesis of 1,4-bis(4-pyridyl)butadiyne. *J. Heterocycl. Chem.* 1984, *21*, 607−608. (b) Amoroso, A. J.; Cargill-Thompson, A. M. W.; Maher, J. P.; McCleverty, J. A.; Ward, M. D. Di-, Tri-, and Tetranucleating Pyridyl Ligands Which Facilitate Multicenter Magnetic Exchange between Paramagnetic Molybdenum Centers. *Inorg. Chem.* 1995, *34*, 4828−4835.

(18) Sheldrick, G. M. SHELXL-2015. *Acta Crystallogr., Sect. C: Struct. Chem.* 2015, *71*, 3−8.